Chapter 13

Earth's Foreshock and Magnetopause

Aims and Expected Learning Outcomes

The **Aims** are to explore the physics of planetary magnetopauses and foreshocks, focusing on the particle motions and their microscopic and macroscopic consequences. Planetary magnetopauses and their associated bow shocks limit entry of the solar wind plasma into the magnetosphere, and thereby affect the physics of the magnetosphere and Earth's space weather. They link solar physics with magnetospheric physics, the next major section of the course.

Expected Learning Outcomes. You should be able to

- Define the foreshock region upstream of a shock and explain the detailed particle motions there.
- Understand and explain qualitatively why bump-on-tail distributions develop and drive plasma waves in foreshock regions.
- Understand and describe the physics of magnetopauses and other current layers, especially their small thicknesses, particle motions, currents, and associated forces and magnetic fields.
- Understand and explain how current layers enable the concept of pressure to be useful in collisionless plasmas, in terms of the currents leading to $\mathbf{J} \times \mathbf{B}$ forces that quantitatively mimic pressure forces.
- Describe and explain the macroscopic current system on the magnetopause, and its role in determining the magnetopause location and affecting magnetic fields at the Earth's surface and elsewhere interior to the bow shock.

13.1 Foreshock Physics

Earth's foreshock is the region upstream from the Earth's bow shock that is magnetically connected to the bow shock and contains both solar wind plasma and also charged particles coming from the bow shock (Figure 13.1). As described in the last Chapter, protons and other solar wind ions specularly reflected from the bow shock have gyrocenter velocities directed into the upstream plasma for $\theta_{Bn} \leq 45$ degrees. These are not the only particles that may stream back into the solar wind from the bow shock. Instead, the following classes of plasma particles can also move into the solar wind from the bow shock:

1. electrons and solar wind ions reflected from the bow shock by magnetic mirroring or scattering by MHD waves,

2. electrons and ions from the magnetosheath can leak back upstream if they can surmount the cross-shock potential and magnetic overshoot.

All charged particles moving in the foreshock, no matter whether they are from the undisturbed solar wind or the bow shock, feel the solar wind's convection electric field and must move with the $\mathbf{E} \times \mathbf{B}$ drift velocity, as well as their parallel velocity and their gyrovelocity. Accordingly, all electrons and ions leaving the bow shock are constrained to lie downstream from the magnetic field line tangent to the bow shock (Figure 13.2). Generalizing Figure 13.1 to consider particle motions in other planes parallel to the plane containing $\mathbf{B}_{sw}$ and $\mathbf{v}_{sw}$, the upstream boundary to the foreshock is the locus of field lines tangent to the bow shock in these planes, while the bow shock comprises the downstream boundary (Figure 13.1).

The $\mathbf{E} \times \mathbf{B}$ drift also causes the development of beam features in particle distributions in the foreshock. This can be seen in Figure 13.1: since the gyrocenters of all particles move in straight lines with $\mathbf{v}_{gc} = \mathbf{v}_{\parallel} + \mathbf{v}_D$, it is clear that particles with larger $v_{\parallel}$ move more nearly parallel to $\mathbf{B}_{sw}$ and are found upstream from particles leaving the same point with smaller $v_{\parallel}$. Put another way, differences in $v_{\parallel}$ lead to dispersion in position. Consider next the parallel speeds of particles reaching a position (R, D_f) in the foreshock, where R and D_f are defined in Figure 13.1. The angle θ is between $\mathbf{v}_{sw}$ and $\mathbf{B}_{sw}$. Simple geometry immediately shows that the minimum speed $v_{\parallel}$ of a particle reaching that point from the bow shock is given by [Filbert and Kellogg, 1979; Cairns, 1987]

$$v_c \approx \frac{R}{D_f \sin\theta} v_D = \frac{R}{D_f} v_{sw} \tag{13.1}$$

with a maximum speed of c. This minimum speed, the "cutoff speed" corresponds to particles reaching (R, D_f) from the tangent point itself. (More exactly, the minimum speed corresponds to particles leaving the shock along a line tangent to the bow shock and passing through (R, x) [Cairns, 1987], but equation (13.1) is a good approximation under most circumstances.) According to Eq. (13.1) and simple geometry, v_c is a strong function of position in the foreshock (Figure 13.3).

Ignoring self-generated wave fields, the particle distribution can be constructed using the Vlasov equation and shown to have a sharp cutoff at $v_{\parallel} = v_c$ (Figure 13.4 below). Qualitatively, this "cutoff" distribution looks like a bump-on-tail distribution and can be expected to drive wave growth via a bump-on-tail instability. The large changes in v_c with position predicted by Eq. (13.1) and Figure 13.3 mean that the beam speed must vary substantially with position in the foreshock.

Before proceeding to describe the plasma waves driven by cutoff distributions in the foreshock, we remark that unstable particle distributions are often produced in space plasmas by such "time-of-flight" effects in which the combination of a localized source of particles and a convection electric field & associated $\mathbf{E} \times \mathbf{B}$ drift (or other plasma drift) leads to constraints on the parallel speed of particles able to reach specified locations. Examples include the magnetosheath, cusp, and plasma sheet in Earth's magnetosphere (Lecture 14), as well as interplanetary travelling shocks and the lunar foreshock.

Figure 13.4 [Fitzenreiter et al., 1990] shows the electron distributions predicted at specific foreshock positions, assuming mirror reflection at the bow shock and the above cutoff effects, while Figure 13.5 shows the observations. The beam-like nature of the predicted distributions is clear in Figure 13.4, while the observations show clear evidence for plateauing of these bump-on-tail distributions (cf. Figure

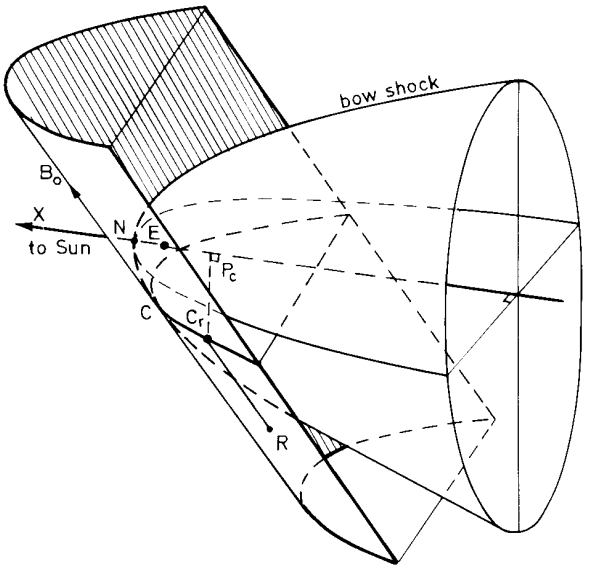

Figure 13.1: Foreshock structure in 3-D [Lacombe et al., 1988].

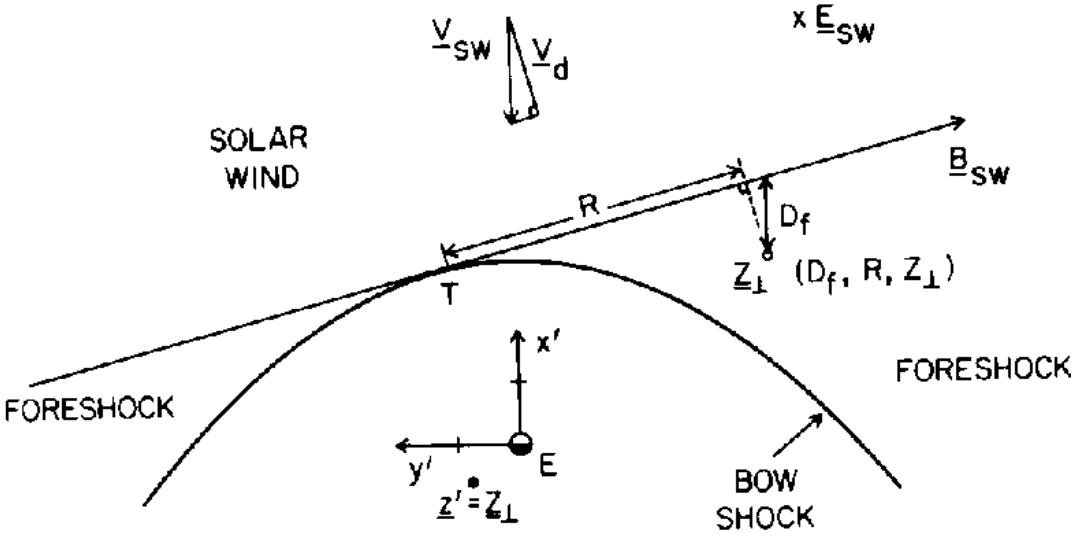

Figure 13.2: The location of the foreshock relative to the bow shock, together with definitions for important coordinates and velocities [Cairns and Robinson, 1999].

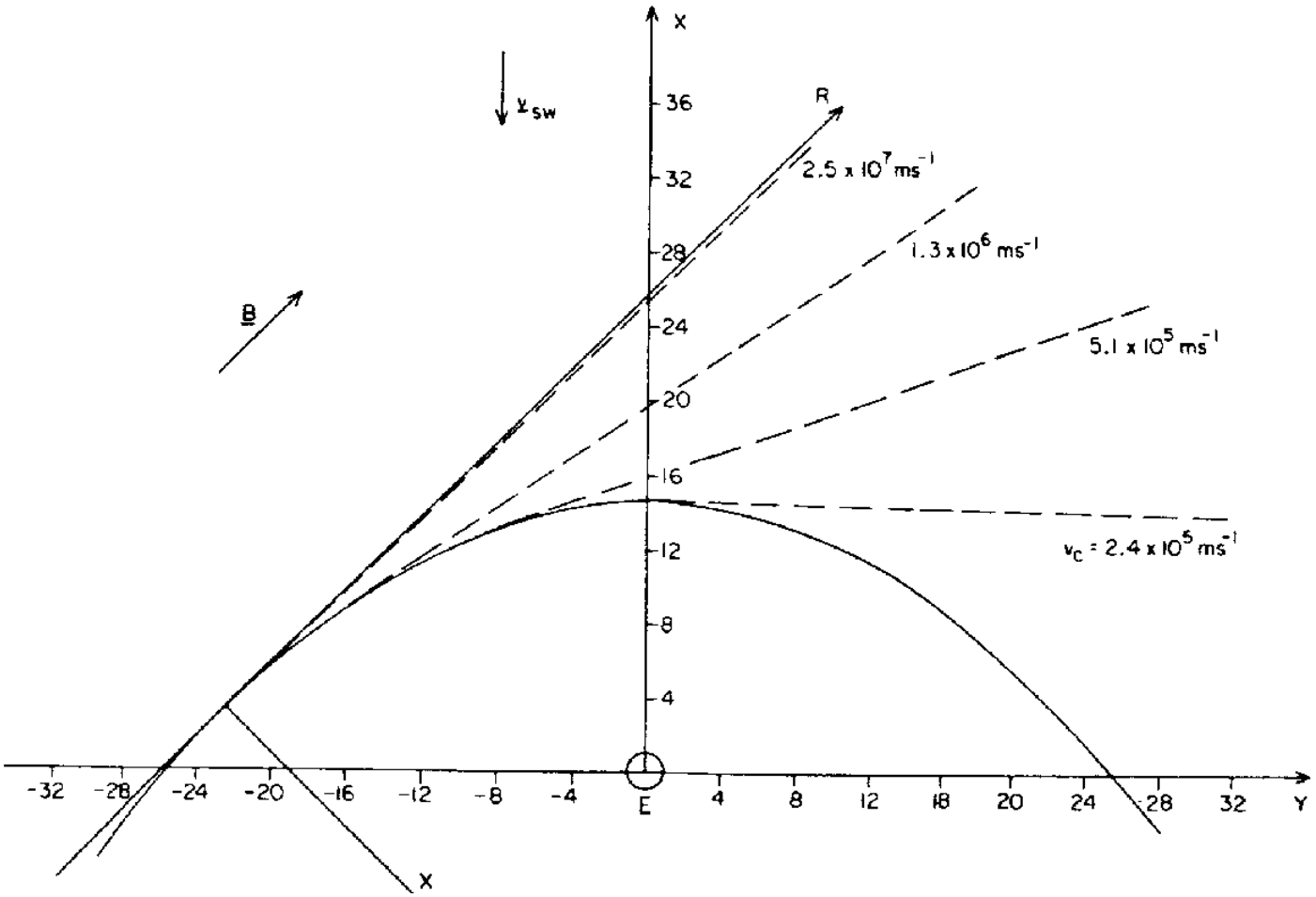

Figure 13.3: Lines of constant v_c in the foreshock [Cairns, 1987], showing that v_c and so the speed of beams varies substantially with position in the foreshock, and that the only regions with large v_c and fast beams are very close to the foreshock boundary.

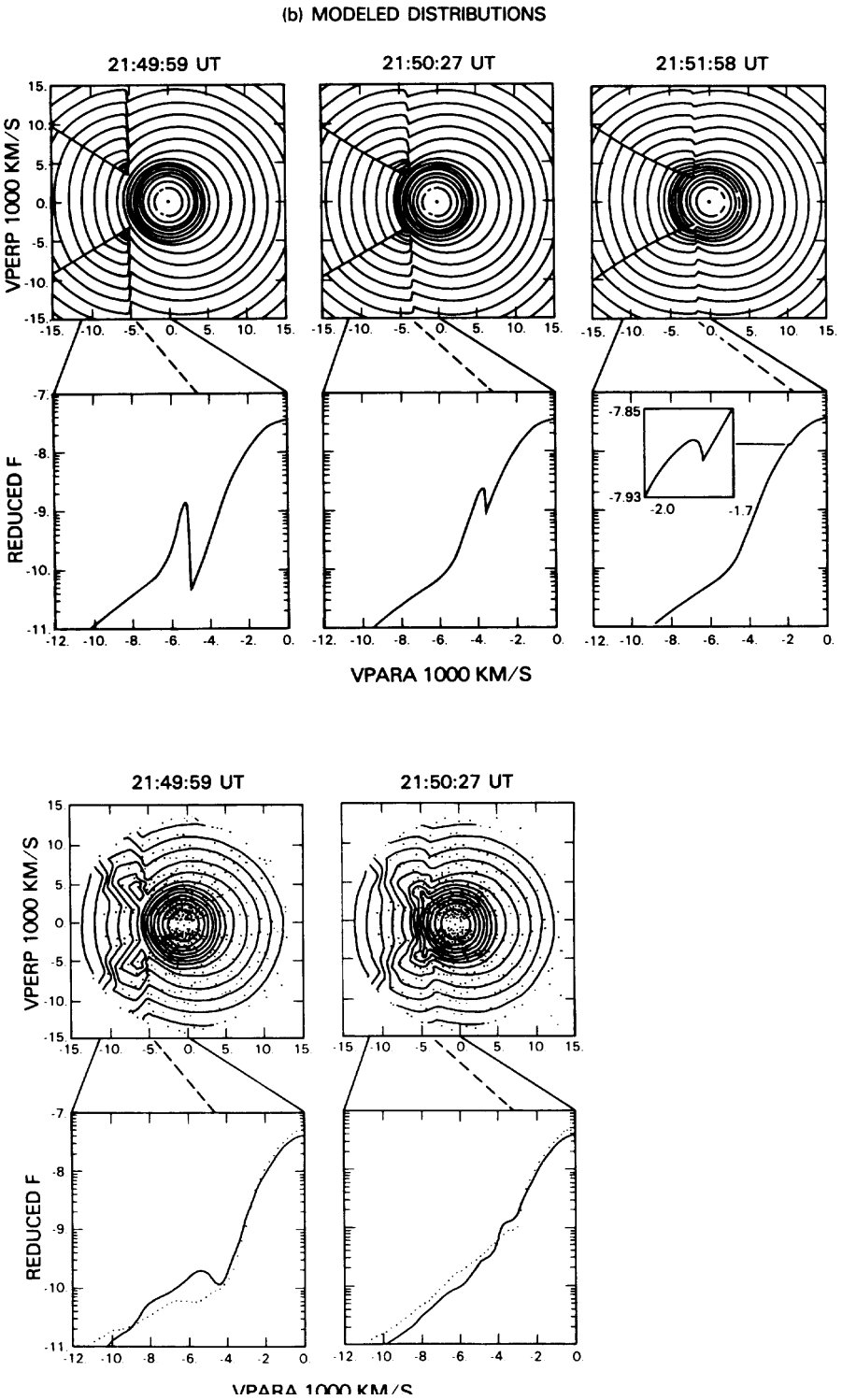

Figure 13.4: Predicted electron distribution functions corresponding to the observations in Figure 13.5 [Fitzenreiter et al., 1990]. These are constructed by following particle paths using the Vlasov / Boltzmann equation with no source/loss terms and including mirror reflection and magnetospheric leakage at the shock. Note the cutoff distribution at v_c and loss cone features. The bottom panels show the effects of limited instrumental resolution.

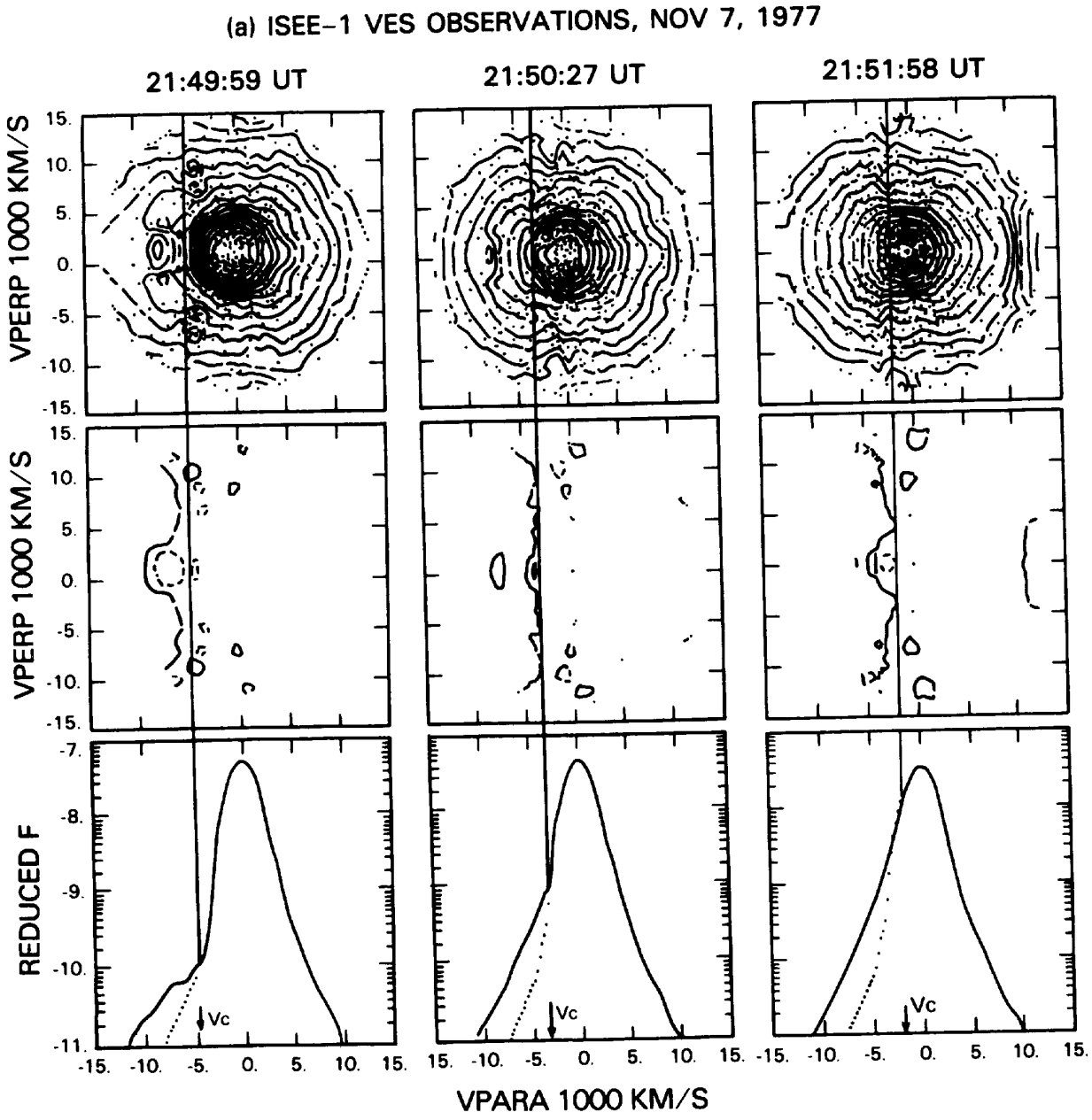

Figure 13.5: ISEE-1 observations near the leading edge of the foreshock (left), deeper in the foreshock (centre) and deep in the foreshock (right) [Fitzenreiter et al., 1990]. The top panels show the 2-D electron distributions, the middle panels the differences $f(v_\parallel, v_\perp) - f_{sw}(v_\parallel, v_\perp)$, and the bottom panels the reduced distributions $f_r(v_\parallel) = \int d^2\mathbf{v}_\perp f(v_\parallel, v_\perp)$. The vertical lines show the predicted value of v_c for the observation location. Beams and loss-cone features are visible, as is very good agreement between v_c and the observed beam speeds.

4.4), presumably due to growth of Langmuir waves and associated quasilinear relaxation. Note that the vertical lines at v_c predicted by Eq. (13.1) show a clear separation between undisturbed solar wind electrons at lower parallel speeds and particles streaming away from the bow shock at higher parallel speeds. The symmetric "horns" in the observed and predicted distributions at significant $v_\perp$ and partial hole in the distribution near $v_\perp = 0$ above v_c are consistent with the formation of a loss cone due to magnetic mirror reflection at the bow shock (cf. Lecture 1). Mirror reflection and associated shock-drift acceleration of these electrons is inferred.

Figure 13.6 illustrates the Langmuir waves excited near $f_p = \omega_p/2\pi$ by cutoff distributions of electrons. This figure also shows radiation generated near $2f_p$, presumably by the same processes that produce similar radio emissions in type III solar radio bursts. Similar data are discussed by Cairns et al. [1997], Lobzin et al. [2005] and papers referenced therein.

Lest you believe that only electron-driven waves are present in the foreshock, let me emphasize that ion beams are also produced by ion reflection at the bow shock. These ion beams drive high levels of ion acoustic waves which are also observed in Figure 13.6. It can be questioned how the "ion acoustic" waves in Figure 13.6 are produced at frequencies of $\sim 1 - 10$ kHz which are much larger than the ion plasma frequency ($\sim$ 0.6 kHz here). The answer is "Doppler shift". The observed wave frequency $\omega' = \omega - \mathbf{k}.\mathbf{v}_{rel}$ where $\mathbf{v}_{rel}$ is the relative velocity between the observer and the wave. In this situation $\mathbf{v}_{rel} \sim -\mathbf{v}_{sw}$ and $v_{sw} \gg V_S$, so that the observed wave frequency is almost entirely Doppler shift. In addition, the ion beams drive high levels of low-frequency MHD waves, both fast mode and Alfven waves. These MHD waves then act as the upstream scattering agents for Fermi acceleration of ions to high energies (cf. Lectures 5 and 11), with the downstream scattering agents being the shock's magnetic mirror and downstream turbulence.

13.2 The Magnetopause

The magnetopause is the thin boundary separating the shocked solar wind plasma from the plasma of the magnetosphere. Interior to the magnetopause, in the magnetosphere, the plasma's motion is dominated by Earth's magnetic field. The magnetopause has a thickness $\sim$ one thermal (magnetosheath) ion gyroradius and it separates a high β, low magnetic field region (the magnetosheath) from the low β, high magnetic field region of the magnetosphere. Here β is defined as the ratio of the plasma's thermal pressure to its magnetic pressure, thereby being expressable as the ratio of twice the sum of the squared ion and electron thermal speeds divided by the Alfven speed squared.

It can be questioned why the magnetopause exists at all: why is there a separation between the magnetosheath and magnetospheric plasmas? The basic reason is that both plasmas have high conductivities and the frozen-in approximations of MHD theory are well satisfied; the corollary of freezing-in one magnetic field is that all other magnetic fields are excluded from the plasma region, thereby requiring the existence of a plasma boundary separating the magnetosheath and magnetospheric plasmas.

Later it will become clear that the magnetopause does not completely separate the magnetosheath and magnetospheric plasmas. This is for several reasons. First, these plasmas are collisionless and non-MHD effects do exist and are important. An illustration of these points is that more energetic particles have larger gyroradii and so are able to traverse thin boundaries which do, however, separate the thermal particles of the two plasmas. Second, magnetic reconnection of solar wind and magnetospheric field lines allows solar wind plasma to enter and primarily

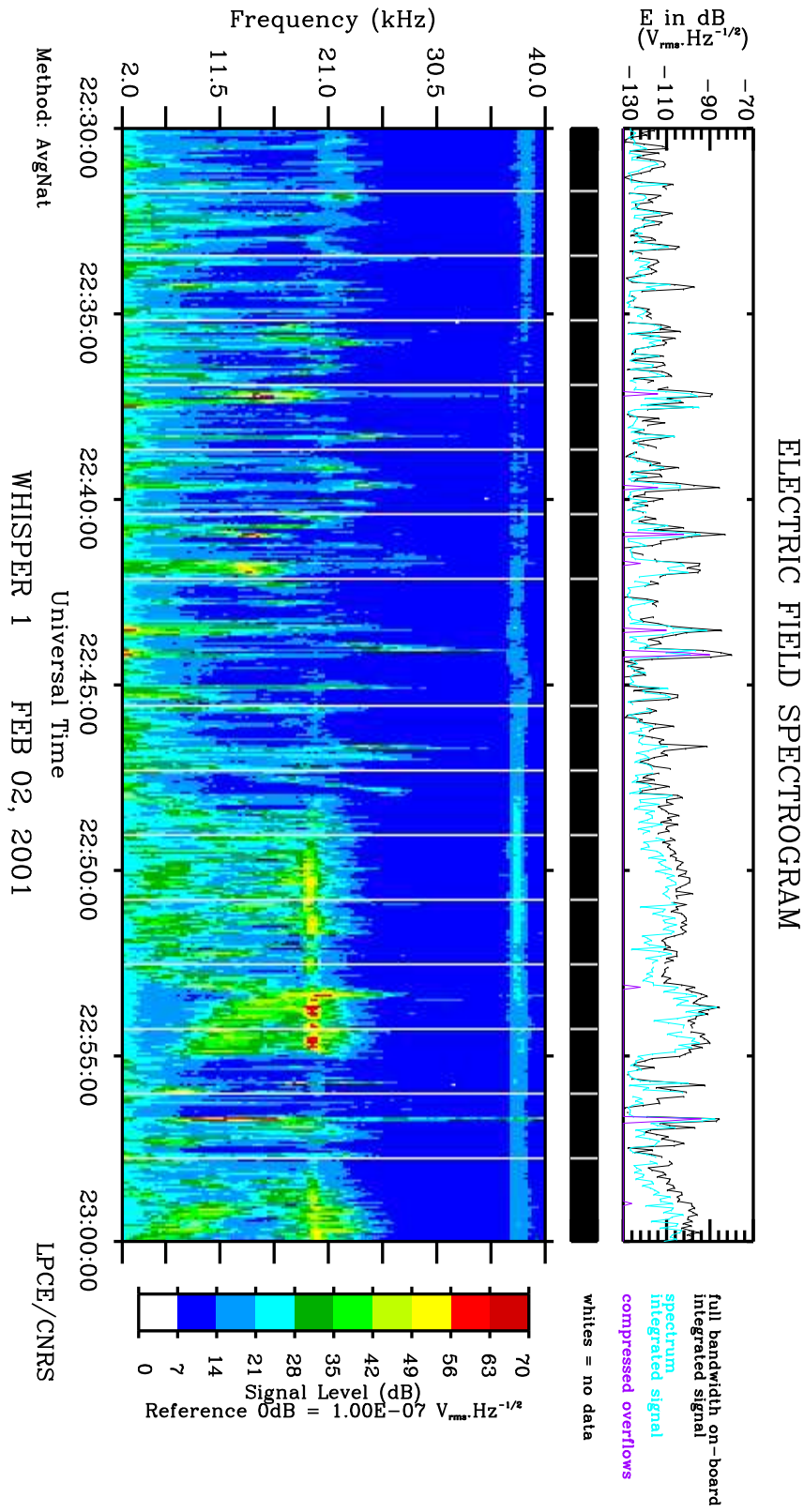

Figure 13.6: Dynamic spectrogram from the Whisper instrument on the Cluster-1 spacecraft, showing intense Langmuir waves in the foreshock near 20 kHz (e.g., 22:50 - 22:55), ion acoustic waves in the foreshock below about 5 kHz, and $2f_p$ radiation generated in the foreshock near 40 kHz. These data are provided courtesy of P. Decreau. See the text for more discussion.

populate Earth's magnetosphere but also allows plasma of terrestrial origin (especially ionospheric ions from the auroral regions and polar caps) to escape from the magnetosphere and enter the solar wind. Magnetic reconnection is considered very important to space weather and the convection of plasma inside Earth's magnetosphere.

As described in Lecture 5, as well as shocks, there are two other types of discontinuities in a collisionless MHD plasma: rotational and tangential discontinuities. Observationally the plasma density, pressure and vector magnetic field vary across the magnetopause, thereby requiring that the magnetopause be a tangential discontinuity. When the magnetopause is stationary it must be in equilibrium with all forces and torques balanced. Frequently this is described in terms of pressure balance, namely that

$$P_{th} + \frac{B^2}{2\mu_0} = \text{constant} \ . \tag{13.2}$$

When the entire solar wind - shock - magnetopause - magnetosphere system is in equilibrium, with the thermal pressure in the magnetosheath ($P_{th,sh}$) equalling the solar wind ram pressure P_{ram} (i.e., neglecting the magnetic pressure there) then

$$P_{th,sh} + \frac{B_{sh}^2}{2\mu_0} = P_{ram} \ . \tag{13.3}$$

It should be recalled (Lecture 2) that the equation of motion for a specific species of charged fluid is

$$\eta \left(\frac{\partial \mathbf{U}}{\partial t} + (\mathbf{U}.\nabla)\mathbf{U} \right) = -\nabla P + \rho \mathbf{E} + \mathbf{J} \times \mathbf{B} \tag{13.4}$$

$$= -\nabla_\perp \left(P + \frac{B^2}{2\mu_0} \right) - \nabla_\parallel P \ + \rho \mathbf{E}. \tag{13.5}$$

The question that should be answered at this stage is how thermal pressure can physically play the role required by Eqs. (13.2) and (13.3) in collisionless plasmas. Put another way, how can the (kinetic) motions of individual particles in collisionless plasmas be reconciled with the role inferred for the pressure in MHD and other fluid theories? It is shown next that the required particle motions lead to currents that then lead to $\mathbf{J} \times \mathbf{B}$ forces that numerically have the magnitudes and functional dependences of the thermal pressure of the plasma. The magnetopause is considered specifically in this example but the results are characteristic and widely applicable. In particular, they apply to pressure-balanced structures in the solar wind and to the heliopause.

Consider a plasma attempting to move from an unmagnetized region into a vacuum region with a magnetic field (Figure 13.7): the thermal electrons and ions both execute approximately half a gyro-orbit before finding themselves back in the unmagnetized region and with velocities directed away from the magnetized region. This leads to the plasma being excluded from the magnetized region. Moreover, notice that the current associated with this partial gyro-orbit is in the same sense for thermal electrons and ions and that the $\mathbf{J} \times \mathbf{B}$ force has the direction required to push the plasma particles out of the magnetized region.

This analysis can be made quantitative. Defining the initial direction of plasma motion as the $\mathbf{x}$ direction, with the $\mathbf{y}$ direction up the page and the magnetic field in the $\mathbf{z}$ direction, the total current for thermal electrons and ions is

$$\mathbf{J} = -\mathbf{y} \left(n_i e v_{\perp,i} + n_e e v_{\perp,e} \right) \ . \tag{13.6}$$

Notice next that the electron current layer is much narrower than the ion gyrolayer, with both having thicknesses of order a gyroradius. Integrating the total current

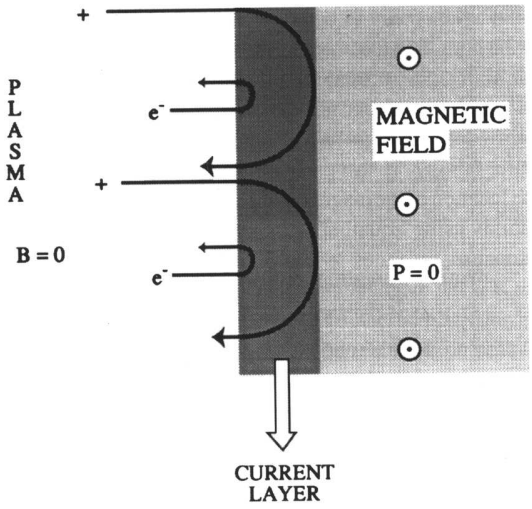

Figure 13.7: Schematic of the current layer which develops as a result of a thermal unmagnetized plasma (left) interacting with a magnetized vacuum region (right) [Cravens, 1997]. The electrons and ions undergo half a gyroorbit in the magnetized region, both species giving rise to a downward current perpendicular to the magnetic field.

over these layers leads to

$$\begin{aligned}
\mathbf{K} &= \int dx \mathbf{J} \\
&= -\mathbf{y}\left(n_i e v_{\perp,i} r_{gi} + n_e e v_{\perp,e} r_{ge}\right) && (13.7) \\
&= -\mathbf{y}\left(n_i \frac{m_i v_{\perp,i}^2}{B} + n_e \frac{m_e v_{\perp,e}^2}{B}\right) && (13.8) \\
&= -\mathbf{y}\left(P_{th,i} + P_{th,e}\right)/B && (13.9)
\end{aligned}$$

for a thermal (Maxwellian) plasma. Thus, integrated in $\mathbf{x}$ over the current layer, the integrated force $\mathbf{J}\times\mathbf{B} = -P_{th}\mathbf{x}$. Put another way, the $\mathbf{K}\times\mathbf{B}$ force naturally balances the pressure force in the fluid momentum conservation equation (2.24). That is, the current in current layers separating kinetic, collisionless plasmas with different properties naturally has the magnitude and direction required for the resultant $\mathbf{J}\times\mathbf{B}$ force to balance the tendency for collisionless thermal plasmas to stream into regions with lower thermal pressure.

The above analysis can be generalized to the case where a cold plasma streams with uniform velocity $v_0\mathbf{x}$ into a region with high magnetic field. In this case the thermal pressure in Eq. (13.9) is replaced by the ram pressure $P_{ram} = n_e(m_i + m_e)v_0^2$. In the case of both a directed motion and thermal motions it is intuitively clear that the effective pressure which the current layer counteracts is the sum of the ram and thermal pressures. Showing these results is left as an Exercise.

These results on current layers explain why the concept of thermal pressure continues to have relevance in collisionless plasmas and also have numerous applications in the solar wind(e.g., pressure-balanced structures, the discontinuities separating shocked solar wind plasmas from CME material, the heliopause) and magnetospheric physics. Of immediate relevance here is the fact that it is the $\mathbf{J}\times\mathbf{B}$ force at the magnetopause current layer which resists the motion of the magnetosheath plasma across the magnetopause, creates a magnetopause obstacle, and

which causes the bow shock to be located well away from the Earth.

The current layer also fulfills another purpose: confining the Earth's magnetic field to the region inside the magnetopause and the (weaker) magnetosheath field to the magnetosheath. Idealizing the magnetosheath to be unmagnetized, it is apparent that the idea of image currents is relevant: an image current flows on the magnetopause so as to remove the Earth's magnetic field from the magnetosheath but also to increase the field strength just inside the magnetopause. This can be seen in Figures 13.8 – 13.10. Numerically, then, the field just inside the magnetopause

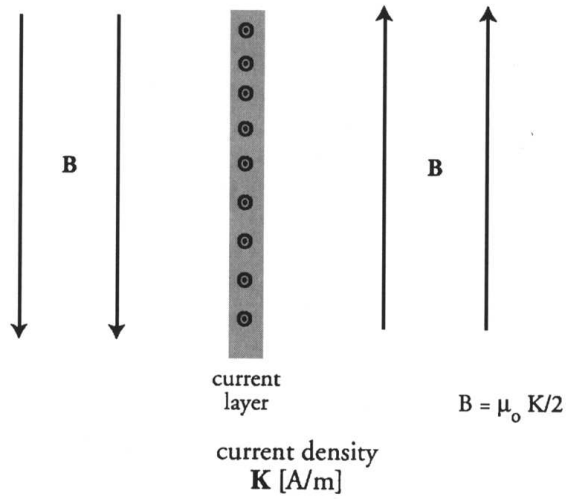

Figure 13.8: Schematic of the magnetic field produced by a current layer with line-integrated current density K [Cravens, 1997].

equals twice the field of the dipole at that distance; that is

$$B_{tot}(r_{mp}) = B_{dip}(r_{mp}) + B_{mp}(r_{mp}) = 2B_{dip}(r_{mp}) \ . \tag{13.10}$$

Balancing the ram pressure of the solar wind against the $\mathbf{J} \times \mathbf{B}$ force and magnetic pressure of the Earth one then has

$$P_{ram} \approx n_{sw} m_i v_{sw}^2 \approx P_{ms} \approx \frac{B_{tot}^2(r_{mp})}{2\mu_0} \ , \tag{13.11}$$

whence

$$r_{mp} \approx \left(\frac{2B_E^2(R_E)}{\mu_0 P_{ram,sw}} \right)^{1/6} R_E \ , \tag{13.12}$$

or about $10R_E$ for typical solar wind conditions (note: $B_E(R_E) = 3 \times 10^{-5}$ T is the dipole magnetic field strength at the Earth's surface). This construction gives the correct location for the magnetopause for normal solar wind conditions. Note that during times of unusually large solar wind ram pressure the magnetopause may move substantially Earthwards. Indeed, sometimes the magnetopause is observed inside geosynchronous orbit ($\sim 6.6R_E$).

The magnetopause current layer is important in two other ways. First, the magnetic field associated with the current layer is also observable at the surface of the Earth. This is particularly true during times when the magnetopause is compressed Earthwards, leading to an increase in the magnetic field measurable at the surface (since the current layer's field adds to the Earth's field inside the magnetopause). As seen in Lecture 15, this effect can lead to an increase in the

geomagnetic activity index D_{st}, often called a Sudden Storm Commencement (SSC), while the increase of the ring current during a geomagnetic substorm leads to a major decrease of the surface field (Chapter 14).

Second, and perhaps more importantly, the magnetopause current layer is a global phenomenon that persists wherever the magnetopause does. How does this global current system close? This is one of the questions pursued in the next three lectures. Figure 13.9 gives a first view of the global nature of the magnetopause current system and the way in which the current loops close. Consistent with Figures 13.8 and 13.9 the magnetopause current is primarily westward near the equator at the front and mid-tail regions of the magnetopause, before turning above/below the magnetic equator (more properly, the tail's current sheet) and closing on the eastward side of the magnetopause. Figure 13.10 shows that the magnetopause currents change direction near the polar cusps discussed more below, flowing primarily eastwards sunwards of the cusps.

The different ion and electron motions in the current layer, and their spatial separation, leads to two other pieces of physics. First, the Hall terms are now important in the MHD equations (e.g., the equations solved should be the Hall-MHD equations) for the current layer itself. Second, the relative streaming of the electrons and ions, and their spatial separation leads to wave instabilities. These instabilities can involve waves with small wavelengths, leading to particle scattering and heating, or they can be on macroscopic rippling and breakup of the current layer. Examples of the latter include Raleigh-Taylor and Kelvin-Helmholtz instabilities.

The final topic discussed now and in Lecture 15 is that of magnetic reconnection at the magnetopause. Suppose that the solar wind magnetic field in Figures 13.9 and 13.10 is directed southwards. Since the dipole field lines are directed northwards this situation involves anti-parallel magnetic field lines being brought together by a plasma flow, thereby suggesting that magnetic reconnection might occur. Magnetic reconnection can lead to magnetosheath and solar wind plasma entering the magnetosphere and magnetospheric plasma escaping into the magnetosheath and solar wind, as well as the creation of accelerated and heated plasma flows and modified magnetic topologies. All these effects are observed. It is perhaps less obvious, but magnetic reconnection is believed to occur sometimes even during times of northward IMF direction and to sometimes involve the east-west components of the magnetic field. These reconnection events occur away from the nose of the magnetopause, near the cusps.

13.3 References and Bibliography

- Cairns, I.H., The electron distribution function upstream from the Earth's bow shock, **J. Geophys. Res.**, **92**, 2315, 1987.
- Cairns, I.H., P.A. Robinson, R.R. Anderson, and R.J. Strangeway, Foreshock Langmuir waves for unusually constant solar wind conditions: Data and implications for foreshock structure, **J. Geophys. Res.**, **102**, 24,249, 1997.
- Cravens, T.E., *Physics of Solar System Plasmas*, Cambridge, 1997.
- Filbert, P.C., and P.J. Kellogg, Electrostatic noise at the plasma frequency beyond the Earth's bow shock, **J. Geophys. Res.**, **84**, 1369, 1979.
- Fitzenreiter, R.J., A.J. Klimas, and J.D. Scudder, Three-dimensional analytical model for the spatial variation of the foreshock electron distribution: Systematics and comparisons with ISEE observations, **J. Geophys. Res.**, **95**, 4155, 1990.

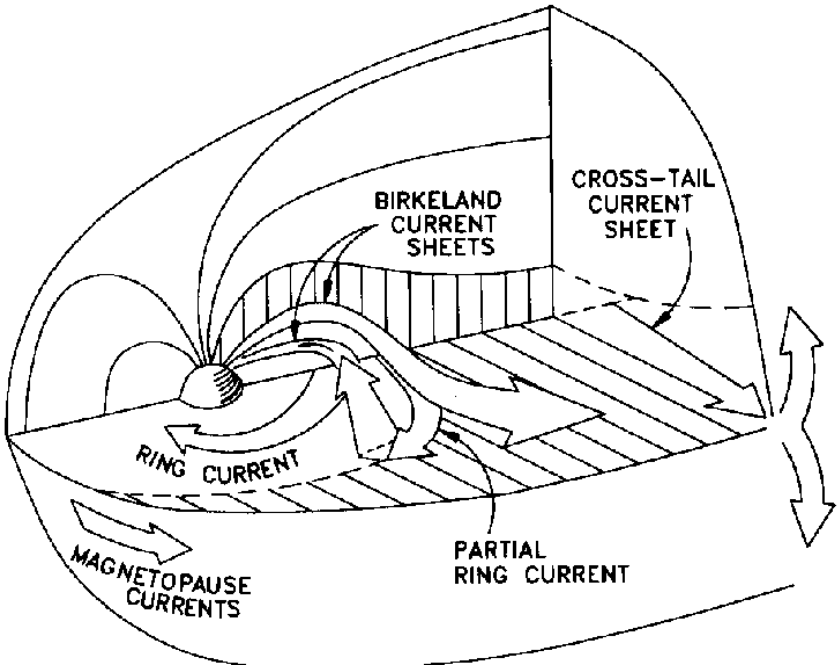

Figure 13.9: The main current systems flowing in Earth's magnetosphere [Stern, 1994], showing the magnetopause current system, ring current, and the cross-tail current. .

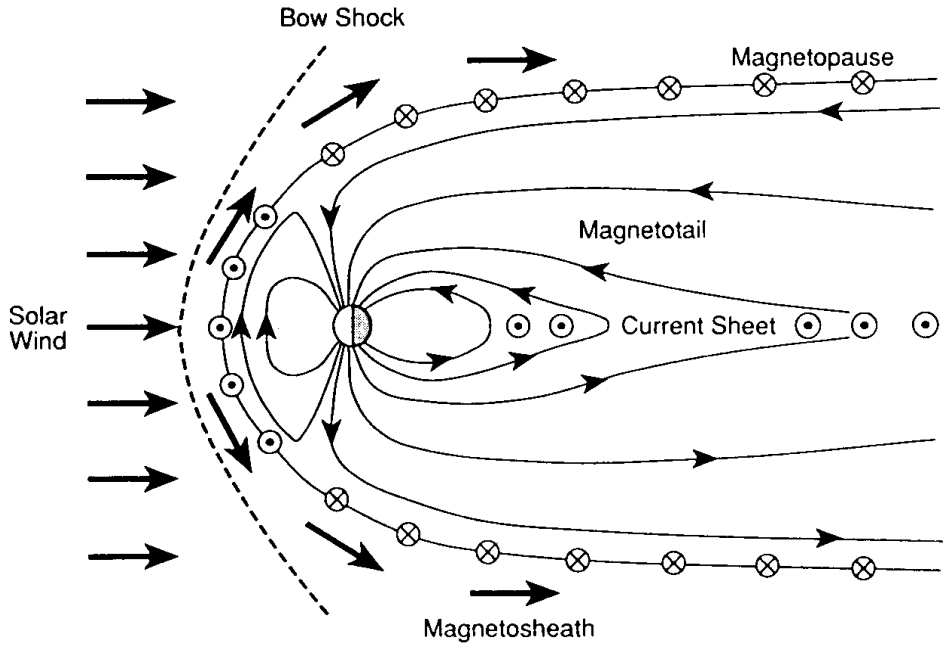

Figure 13.10: Cross section of the global magnetosphere, showing the magnetopause current system, the cusps, the magnetotail, and the magnetotail current sheet [Hughes, 1995].

- Gosling, J.T., M.F. Thomsen, S.J. Bame et al., Evidence for specularly reflected ions upstream from the quasi-parallel bow shock, **Geophys. Res. Lett.**, **9**, 1333, 1982.

- Greenstadt, E.W., and R.W. Fredricks, Shock systems in collisionless space plasmas, in *Solar System Plasma Physics Vol. III*, Eds L.J. Lanzerotti, C.F. Kennel, and E.N. Parker, North-Holland, 3, 1979.

- Hughes, W.J., The magnetopause, magnetotail, and magnetic reconnection, in *Introduction to Space Physics*, Eds M.G. Kivelson and C.T. Russell, Cambridge, 1995.

- Lobzin, V., V.V. Krasnoselskikh, S. Schwartz, I.H. Cairns, B. Lefbvre, and P. Decreau, Generation of downshifted oscillations in the electron foreshock: A loss-cone instability, Geophys. Res. Lett., 32(18), CiteID L18101, 2005.

- Stern, D.P., The art of mapping the magnetosphere, **J. Geophys. Res.**, **99**, 17,169, 1994.